Supplemental Information

Supplemental Data

Supplemental Results

Polysome-profiling and ribosome-profiling to define effects of TIF4631-VPS35 on translation initiation

Our data are consistent with the hypothesis that TIF4631 upregulation causes alterations in translation in the absence of VPS35, which could lead to protein misfolding and impairments in sortilin to cope with these misfolded proteins. To test this hypothesis, we next measured protein synthesis directly by performing polysome-profiling experiments (Figure S3). This technique involves fractionation, by differential centrifugation, and quantification of the relative abundance of different populations of translating ribosomes – creating a polysome profile, which provides an estimate of protein synthesis. Alterations in the polysome profile indicate changes or defects in translation initiation (Coudert et al., 2014). We found a striking reduction in the amount of polyribosomes relative to monoribosomes in *vps35*Δ cells upregulating TIF4631 compared to control cells (WT, *vps35*Δ, or WT cells upregulating TIF4631; Figure S3A). Thus, upregulation of TIF4631 causes a specific impairment in translation initiation in the absence of VPS35.

Because both eIF4G1 and VPS35 have broad cellular functions (translation initiation and vesicle trafficking, respectively), we next used ribosome profiling to investigate in more detail the specific molecular networks that might connect these genes. This technique enables genome-wide assessment of translation at high resolution because it utilizes deep sequencing of ribosome-protected mRNA fragments (Ingolia et al., 2009). The amount of ribosome-protected fragments (footprints) within the coding region of an open reading frame correlates with the amount of protein produced. We performed ribosome profiling to define which genes showed differential translation in each genetic background (Figure S3B). Interestingly, we did not observe widespread changes in translation of many genes. Rather, we found a small number of functionally related genes that had altered translational profiles upon TIF4631 upregulation (Figure S3B). For

example, upregulation of TIF4631 in WT cells caused an increase in translation of four critical yeast biotin biosynthetic genes (BIO2, BIO3, BIO4, and BIO5). This increase in biotin biosynthetic gene expression was attenuated in the absence of VPS35 (Figure S3B). Could the specific downregulation of one or more of these biotin genes in *vps35*Δ cells contribute to their sensitivity to TIF4631 upregulation? To test this, we attempted to rescue TIF4631 toxicity in *vps35*Δ by co-expressing five separate biotin genes present in our plasmid library. Overexpression of BIO4 alone was sufficient to partially rescue the toxicity of Tif4631 overexpression (Figure S3C). Taken together, these first steps into better understanding the molecular networks connecting TIF4631 and VPS35 will hopefully open up interesting avenues of further experimentation, with the goal to define disease relevant translational targets of EIF4G1 and to see how these may be altered in human disease.

Human postmortem analysis of VPS35, EIF4G1 and α–syn

To extend our findings from model systems to human disease, we next investigated connections between VPS35, EIF4G1 and α-syn by analysis of human patient postmortem tissue. We measured protein levels and subcellular distributions by immunoblot. Compared to controls, in patients with dementia with lewy bodies (DLB) or Parkinson's disease (PD) the cytosolic to membrane ratio of VPS35 was altered with less VPS35 in the cytosol and more in the membrane fraction (Figure S4 A,C). The EIF4G1 ratio was also altered, but in the opposite manner: increased EIF4G1 in the cytosol and less in the membrane fraction in the DLB/PD cases compared to controls (Figure S4 B,D). The DLB/PD samples also displayed increased accumulation of α-synuclein monomer and oligomers in the membrane fraction and a slight increase in Rab5, a marker of early endosomes (Figure S4 A,C). Consistent with these findings, the cytosolic/membrane ratio of VPS35 was reduced and the EIF4G1 ratio was increased in the brains of α-synuclein transgenic mice compared to controls (Figure S4 B,D). Thus, VPS35 and EIF4G1 protein levels and subcellular localization are abnormal in a mouse synucleinopathy model and in human disease.

We also analyzed the distribution and localization of VPS35 and EIF4G1 in human brain vibratome sections of the frontal cortex and non-tg and α-syn tg mice by

immunocytochemistry. Both proteins located to granular structures in the cytoplasm and in DLB/PD patients there was a less marked granular appearance and instead the immunostaining was more diffuse (Figure S4 E,F). We used double labeling and laser scanning confocal microscopy to assess co-localization between VPS35 and EIF4G1 in human brain and in non-tg and α-syn tg mice. In the control human brains and non-tg mice VPS35 and EIF4G1 co-localized in granular structures in the cytoplasm, whereas in the DLB/PD and α-syn tg mice there was markedly less co-localization (Figure S4 G,H) .

To better understand the role of alterations in VPS35 in α-synucleinopathies we generated lentiviral vectors expressing WT, P316S and D620N VPS35 and well as shVPS35 tested in a neuronal cell line (B103) and in the brains of non-tg and tg mice (Figure S5). By immunoblot, compared to controls, the WT and mutant lentiviruses expressed VPS35 at about one fold higher than the levels of the control; the levels were comparable between the WT and mutant constructs. In contrast, with the shRNA there was a 95% reduction in the expression of VPS35. Similar results were observed by immunocytochemical analysis. In non-tg mice, 4 weeks after injection of the LV-control in the hippocampus, low to moderate levels of VPS35 were detected. In contrast injection of LV-WT or mutant VPS35 resulted in a significant 2-3-fold increase, while with shRNA VPS35 there was a significant 90% reduction (Figure S5).

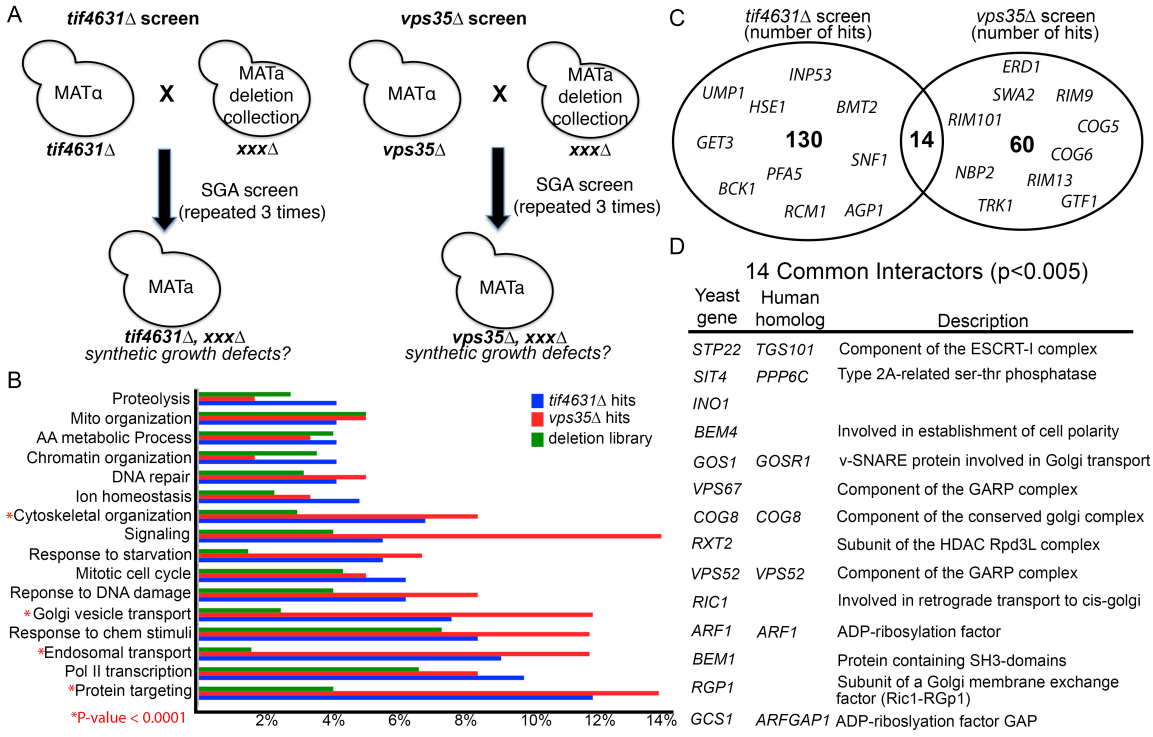

Yeast gene	Human homolog	Description
STP22	*TGS101*	Component of the ESCRT-I complex
SIT4	*PPP6C*	Type 2A-related ser-thr phosphatase
INO1		
BEM4		Involved in establishment of cell polarity
GOS1	*GOSR1*	v-SNARE protein involved in Golgi transport
VPS67		Component of the GARP complex
COG8	*COG8*	Component of the conserved golgi complex
RXT2		Subunit of the HDAC Rpd3L complex
VPS52	*VPS52*	Component of the GARP complex
RIC1		Involved in retrograde transport to cis-golgi
ARF1	*ARF1*	ADP-ribosylation factor
BEM1		Protein containing SH3-domains
RGP1		Subunit of a Golgi membrane exchange factor (Ric1-RGp1)
GCS1	*ARFGAP1*	ADP-riboslyation factor GAP

Figure S1, related to Figure 1. Yeast synthetic lethal screens with *vps35*Δ and *tif4631*Δ enrich overlapping categories of genes. A) Schematic representing synthetic lethal screens for *vps35*Δ and *tif4631*Δ using synthetic genetic array (SGA) resulting in an arrayed collection of double deletions (e.g., *vps35*Δ *xxx*Δ or *tif4631*Δ *xxx*Δ) that were assessed for growth. B) Functional categories of genes enriched as synthetic sick or lethal hits in the *vps35*Δ (red bars) and *tif4631*Δ (blue bars) screens compared to the frequency of those categories in the non-essential deletion mutant collection (green bars). C) Venn diagram showing the number of genes from the deletion collection that genetically interact with *vps35*Δ or *tif4631*Δ. The top nine strongest genetic interactors from the *vps35*Δ and *tif4631*Δ are listed. All genetic interactors are listed in Table S1. D) List of genes that interact with both *vps35*Δ and *tif4631*Δ.

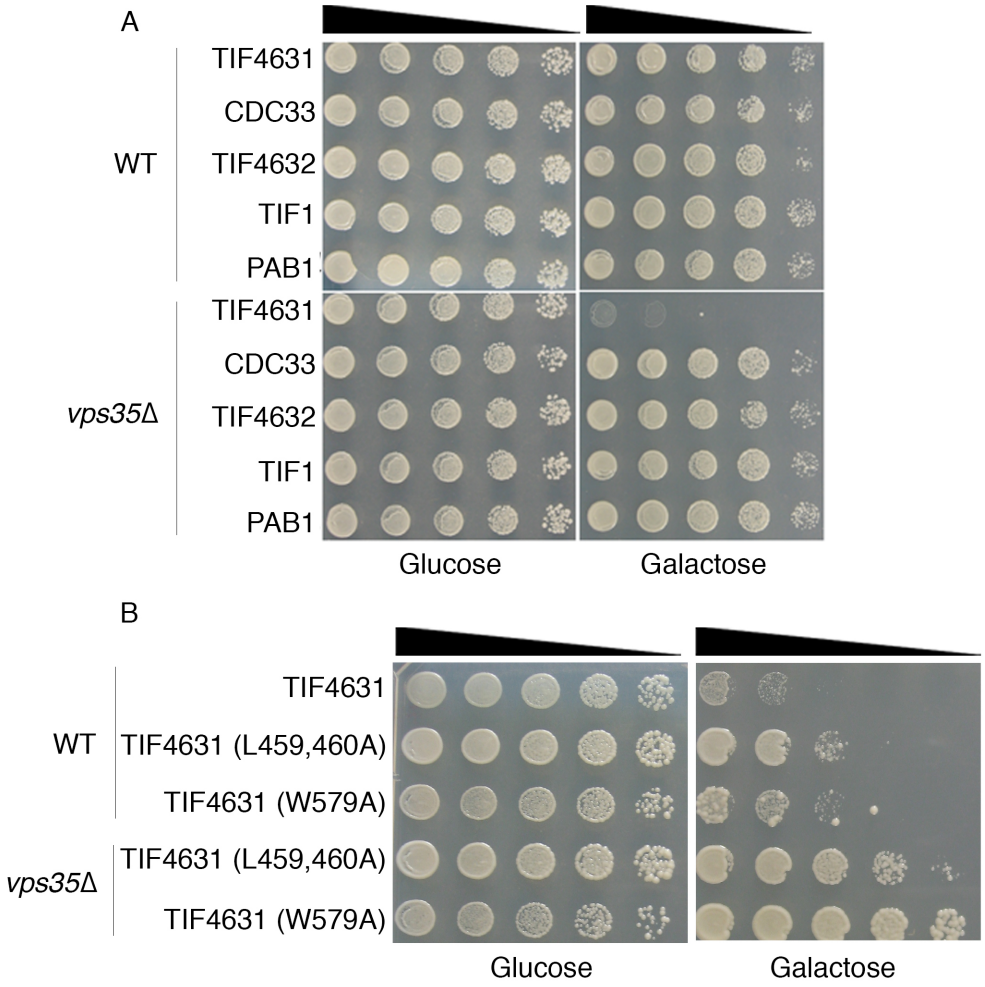

Figure S2, related to Figure 1. Specificity of TIF4631-VPS35 genetic interaction. A) Upregulation of TIF4631 has no effect on growth in WT cells but is highly toxic in *vps35*Δ cells. This effect is specific to this translation initiation factor because upregulation of four other translation initiation factors, including TIF4632, does not cause this synthetic toxicity in *vps35*Δ cells. B) The effects of TIF4631 in vps35Δ cells depends on translation because specific mutations in TIF4631 that interfere with its association with eIF4E (L459,460A) or eIF4A (W579A) and therefore impair its function in translation initiation are less toxic in *vps35*Δ cells than WT TIF4631.

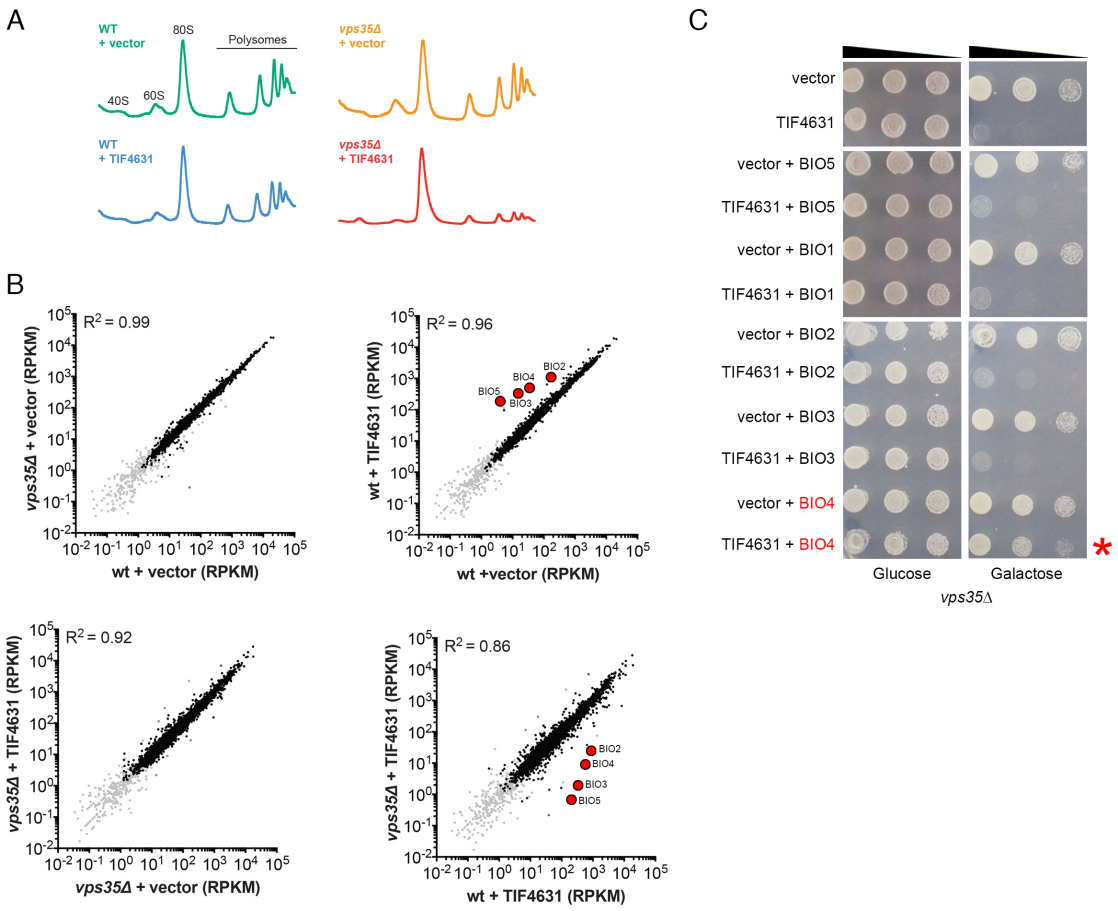

Figure S3, related to Figure 3. Polysome- and ribosome-profiling to investigate effects of TIF4631 and VPS35 on translation initiation. A) Polysome-profiling experiment to measure ribosome abundance in different genetic backgrounds. Ten OD_{600} units of yeast lysates were separated by ultracentrifugation through a 7−47% sucrose gradient and monitored by OD_{254}. The 40S, 60S, and 80S monosome peaks are labeled as well as the peaks corresponding to polysomes. TIF4631 upregulation in *vps35*Δ caused a decrease in polysomes, indicating decreased translation initiation. B) Ribosome-profiling experiment to compare translation of mRNAs in WT, *vps35*Δ, TIF4631 expressing, and *vps35*Δ + TIF4631 expressing backgrounds. Comparison of total open read frame reads between pairs of datasets. Reads within each open reading frame, excluding the first two and last two codons, are summed, and then divided by the adjusted length of the gene and the total reads for the dataset to give reads per kilobase per million (RPKM). Open reading frames for which there are fewer than 128 total reads shared between datasets are shaded gray and are excluded from the calculation of correlation. TIF4631 expression caused an

upregulation in four biotin genes in WT cells (upper right plot) but these genes were downregulated in *vps35*Δ overexpressing TIF4631 (bottom right plot). Biotin genes are highlighted in red on each plot. C) Yeast spotting assay to test ability of biotin genes (BIO1, BIO2, BIO3, BIO4, or BIO5) to rescue TIF4631 toxicity in *vps35*Δ. Upregulation of BIO4 (highlighted in red) was sufficient to partially rescue the TIF4631-induced growth defect.

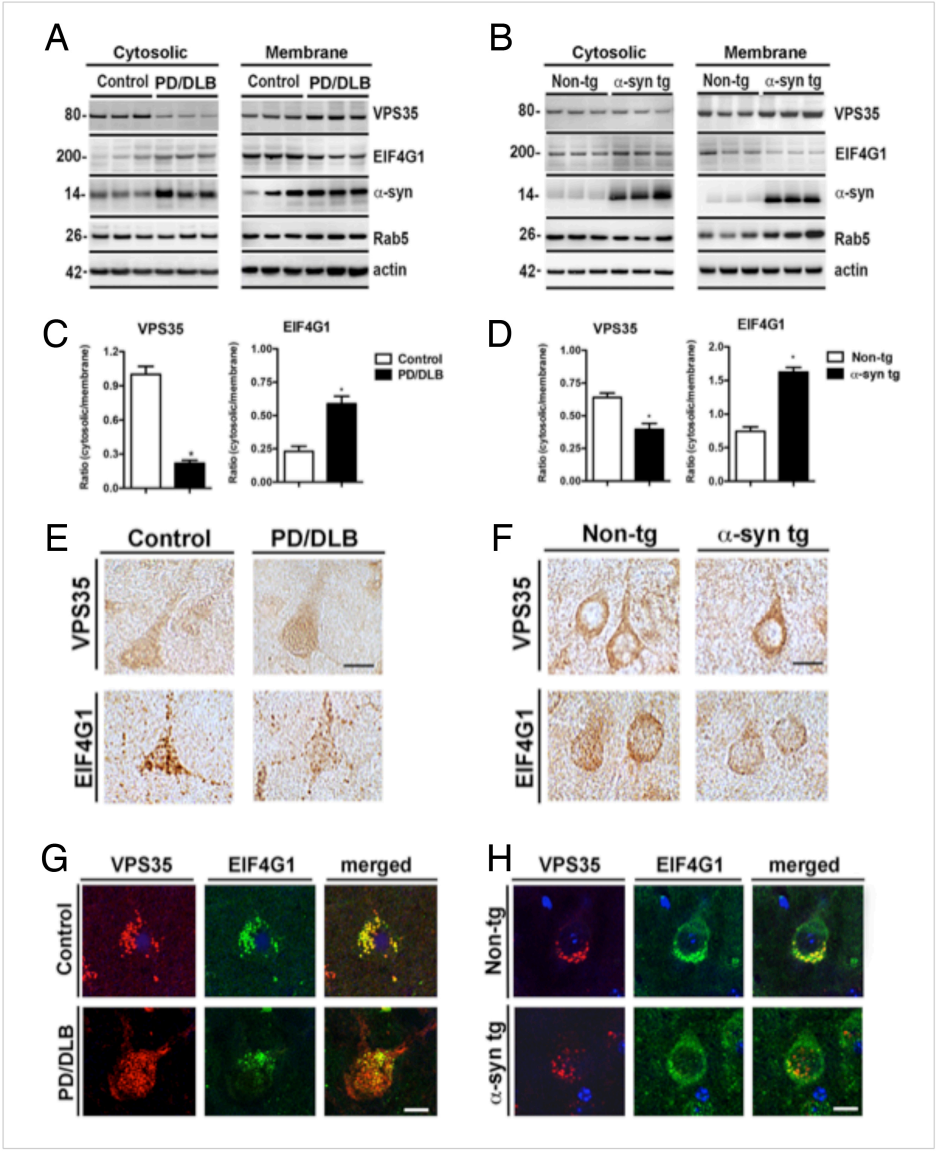

Figure S4, related to Figure 5. Alterations in VPS35 and EIF4G1 in DLB/PD and α-syn transgenic mouse brains. A) Immunoblot analysis in the cytosolic and membrane fractions from the frontal cortex of control and DLB/PD brains. VPS35 (80 kDa), EIF4G1 (200 kDa), α-syn (14 kDa), Rab5 (26 kDa) and β-actin (42 kDa) were analyzed. B) Identification of VPS35, EIF4G1, α-syn, Rab5 and β-actin in the cytosolic and membrane fractions in non-tg and α-syn transgenic (tg) mice. C,D) Densitometric analysis of the ratio of cytosolic to membrane fraction for VPS35 and EIF4G1 in human brains and transgenic mice, respectively. E,F) Immunocytochemical analysis of the distribution and localization of VPS35 and EIF4G1 in human brain vibratome sections for the frontal cortex and non-tg and α-syn tg mice showing that both of these markers

are located in granular structures in the cytoplasm, in DLB/PD patients there is a less marked granular appearance and instead the immunostaining is more diffuse. G,H) Double labeling and laser scanning confocal microscopy analysis of co-localization between VPS35 and EIF4G1 in human brain vibratome sections for the frontal cortex and non-tg and α-syn tg mice. In the control human brains and non-tg mice VPS35 and EIF4G1 are co-localized in granular structures in the cytoplasm, whereas in the DLB/PD and α-syn tg mice there is less co-localization. n=6 control and n=6 DLB/PD or n=6 non-transgenic and n=6 α-syn transgenic mice. *= <0.05 by un-paired, Student's T test.

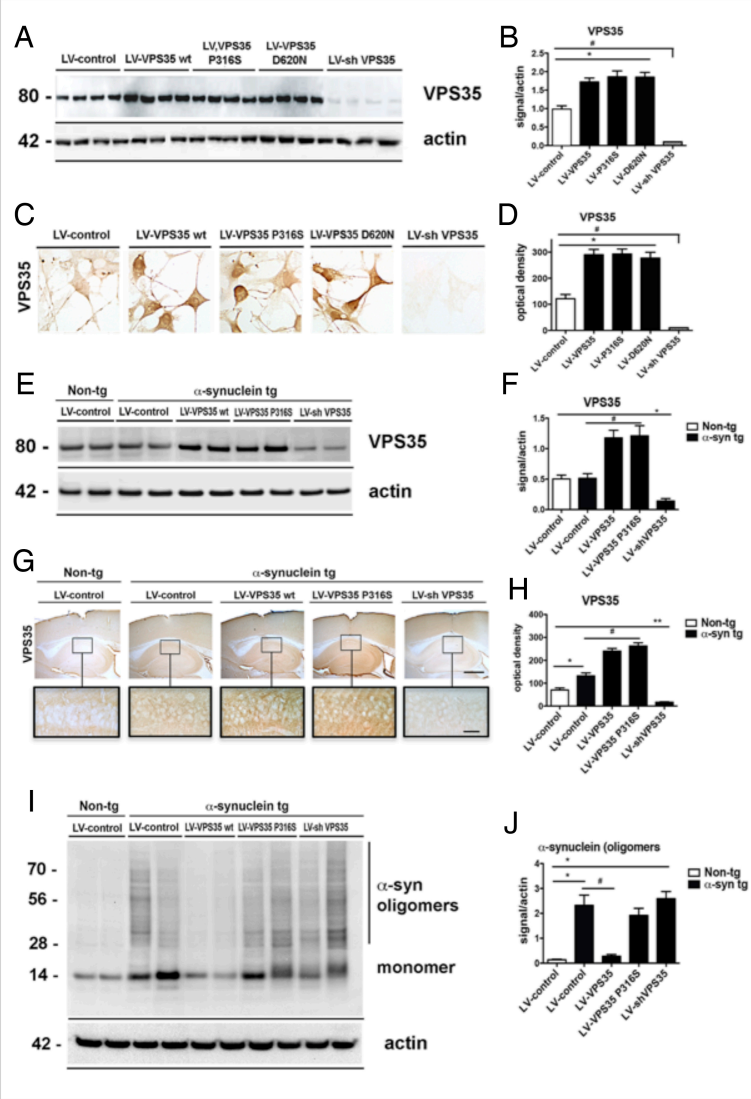

Figure S5, related to Figure 5. Validation of lentiviruses expressing VPS35 and shRNA. A) Immunoblot analysis in the membrane fractions from neuronal cells infected at MOI 40 with LV-VPS35 wt, PD-associated mutants or VPS35 shRNA. B) Densitometric analysis of VPS35 levels compared to actin levels. C) Immunocytochemical analysis of VPS35 immunostaining in B103 neuronal cell lines 48 hrs after lentivirus infection. D) Image analysis of levels of VPS35 immunoreactivity following infection with lentiviruses. E) Immunoblot analysis of levels of VPS35 in the brains of control and tg mice injected with VPS35 lentiviruses, F) Densitometric analysis of α-syn levels compared to actin levels. G) Immunocytochemical analysis of VPS35 immunostaining in the brains of non-tg and α–syn tg mice 4 weeks after injection of VPS35 wt, mutant and shRNA infection into the hippocampus. Image in box represents higher magnification of the marked area.

H) Image analysis of levels of VPS35 immunoreactivity following injection with lentiviruses into the hippocampus. Bar=250 um (low power view) and 50 um (box). I) Immunoblot analysis of levels of α-syn in the brains of control and tg mice injected with VPS35 lentiviruses, J) Densitometric analysis of α-syn levels compared to actin levels. n=6 non-tg and n=6 α-syn tg mice. *= <0.05 by one way ANOVA with Dunnett's post hoc test when comparing control to LV-VPS35 and # when comparing control to shVPS35.

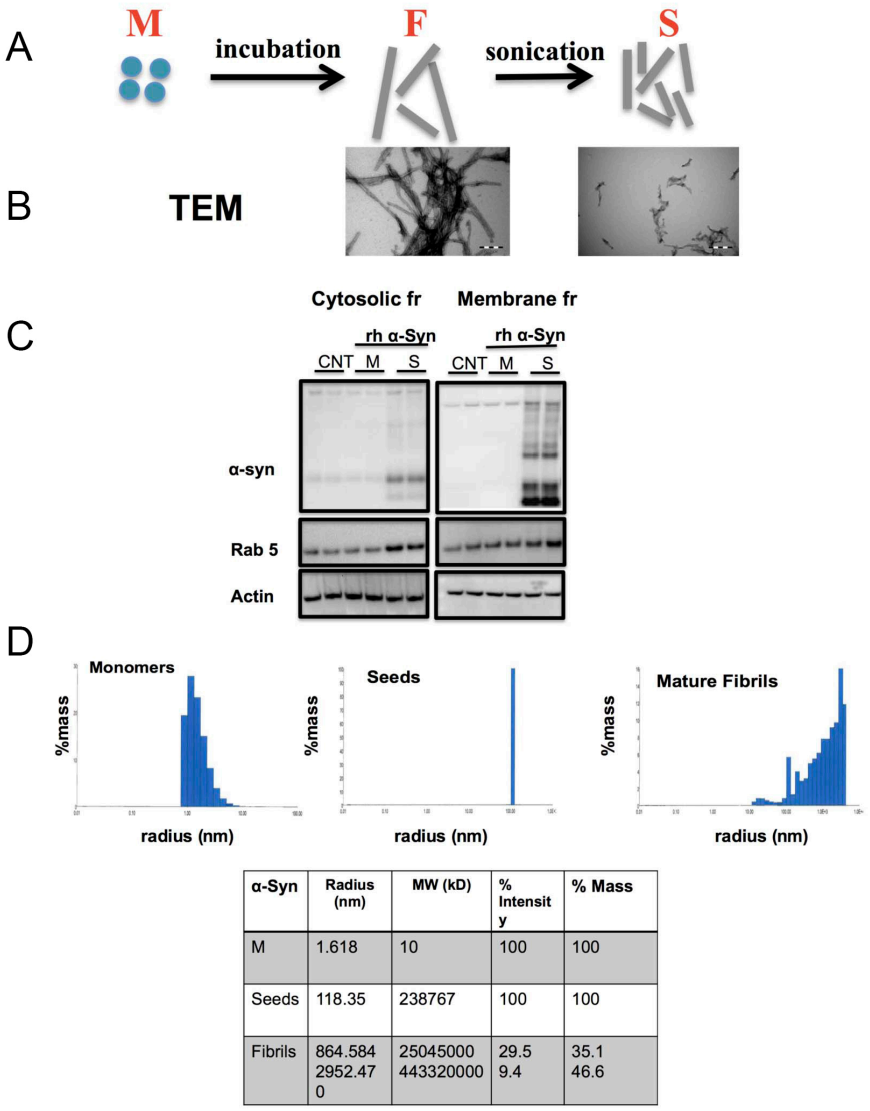

α-Syn	Radius (nm)	MW (kD)	% Intensity	% Mass
M	1.618	10	100	100
Seeds	118.35	238767	100	100
Fibrils	864.584 2952.470	25045000 443320000	29.5 9.4	35.1 46.6

Figure S6, related to Figure 5. Characterization of human recombinant exogenous α-syn seeds. A) Process of seeds preparation. Human recombinant α-syn (hr α-syn) monomers (M) were incubated for 72 hours to obtain mature fibrils (F) and then seeds (S) were generated by sonication of mature fibrils. B) Fibrils and seeds were also characterized by transmission electron microscopy (TEM). C) Uptake of α-syn monomers and α-syn seeds was been detected by immunoblot of cytosolic and membrane fractions of cortical neurons. D) α-Syn monomers, seeds and fibrils were also analyzed by Dynamic Light Scattering (DLS). Purity of monomers, seeds and fibrils preparation was analyzed following the percentage of mass (% mass) and radius of the different species. The table indicates values for these three α-syn species.

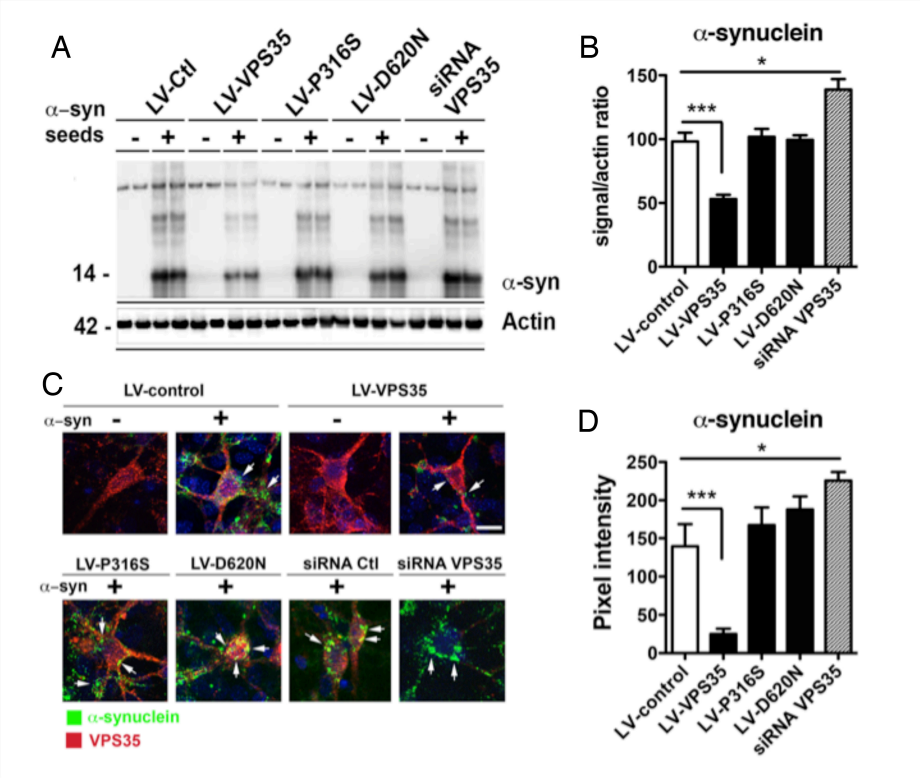

Figure S7, related to Figure 5. VPS35 upregulation mitigates the accumulation of exogenous α-syn seeds in cortical neurons. Cortical neurons were infected with lentivirus VPS35 (LV-VPS35), lentivirus VPS35-P316S (LV-P613S) or VPS35-D620N (LV-D620N), or transfected with siRNA anti-VPS35 (siRNA VPS35) and exposed to 1μM of exogenous α-syn seeds (+) to evaluate the effect of VPS35 modulation on the uptake and accumulation of exogenous α-syn seeds. A) Immunoblot analysis α-syn (14kD) and β-actin (42kD) levels in membrane fractions of cortical neurons in VPS35 modulation. B) Exogenous α-syn seeds levels were quantified in cortical neurons by densitometric analysis and normalized to β-actin levels. C) Double immunolabeling of VPS35 (red) and α-syn (green) proteins in cortical neurons to evaluate the uptake of exogenous α-syn seeds upon VPS35 modulation. Arrows indicate the uptake of seeds by the neurons. D) Levels of accumulated α-syn seeds were quantified in cortical neurons by densitometric analysis and normalized to β-actin levels.

Supplemental Experimental Procedures

Preparation of recombinant α-syn seeds

Human recombinant α-synuclein (h recombinant α-syn, rPeptide) was dissolved in Tris 10mM, 150 mM NaCl pH=7.6 (1mg/mL) for 72 hours in agitation at 37 °C to obtain mature fibrils. The fibrils were monitored by ThT assay, Electon Microscopy (EM) and Dynamic Light Scattering (DLS). To generate seeds (short fibril, around 200nm of lenght), the mature fibrils were ultrasonicate 20 times (pulse, 5 seconds on and 5 seonds off) at amplitude of 40 watts

Polysome profiling

Yeast cells were grown in minimal media with raffinose to mid-log phase. Galacotose (final concentration of 2%) was added to the growth media to induce gene expression from plasmids for 4 hours. Cells were harvested by fast-filtration and flash frozen in liquid nitrogen. Lysis buffer (20 mM potassium HEPES pH 7.5, 150 mM potassium acetate, 10 mM magnesium acetate, 100 µg/ml cycloheximide, 1 mM DL-dithiothreitol, 20 U/ml SUPERase·In (Ambion), cOmplete EDTA-free protease inhibitor cocktail (Roche), 1% Triton-X 100) was frozen drop-wise and then combined with cells. The cells were disrupted using a MM-301 mixer mill (Retsch). Lysates were clarified by centrifugation at 13,000 × g for 10 minutes. Lysate concentrations were normalized using absorbance at 260 nm. Samples were separated over a 7% to 47% sucrose gradient (in lysis buffer with 0.01% Triton-X 100) by ultracentrifugation using a Beckmen SW41 Ti rotor for 2.5 hours at 39,000 rpm. Polysome profiles were recorded using an Isco UA-6 detector.

Sequencing of ribosome protected mRNA footprints

Lysates were prepared as for polysome profiles except cells were disrupted using digest buffer (20 mM Tris pH 7.5, 140 mM KCl, 1.5 mM $MgCl_2$, 100 µg/ml cycloheximide, 1% Triton X-100). Lysates were digested with RNase I (Ambion) for 1 hour at room temperature. Reactions were stopped by the addition of SUPERase·In and ribosomes were immediately pelleted through a 35% sucrose cushion (with 20 mM Tris-HCl, pH 7.5,

140 mM KCl, 5 mM $MgCl_2$, 100 µg/ml cycloheximide, 20 U/ml SUPERase·In) by ultracentrifugation in a Beckman MLA-130 rotor for 4.5 hours at 70,000 rpm. Total RNA was extracted from the pellet using a miRNeasy mini kit (Qiagen). Sequencing libraries were prepared as previously described (Ingolia et al., 2012). After cDNA circularization, ribosomal sequences were depleted using 5′-biotinylated DNA oligonucleotides (sequences available upon request).

PCR amplified libraries were quantified by qPCR (Kapa biosciences), and sequenced using a HiSeq 2500 (Illumina).

Processing and alignment of sequencing reads

Low-quality reads were discarded and adapter sequences were trimmed from the 3′ end of reads. The S. cerevisiae S288C reference genome sequence, release 64, was obtained from www.yeastgenome.org. Alignments were performed using Bowtie 2 (Langmead, 2012). Reads were first aligned to a library of yeast ribosomal RNA. Unaligned reads were then aligned to a library of the coding strands of non-dubious ORF coding sequences including 21 nt flanking upstream and downstream. Genes for which at least 20% of mapped footprints had multiple possible alignments were omitted. For each read length ranging from 23 to 33 nt, codon positions were approximated by determining the center point of the read and applying an empirically determined correction factor so that mean normalized plots (calculated described in (Drost et al., 2013)) showed 3 nt periodicity, with the prominent start codon peak maximized at position 2 (i.e. A**T**G). Reads were then summed for each codon.

Determination of translation levels

Total expression levels were determined by summing all reads within considered coding sequences, omitting the first two and last two amino acid-encoding codons. Thus reads originating from initiation and termination complexes were excluded. For each gene, expression level was calculated by dividing coding sequence reads by the dataset total expression reads, the length of the gene in kilobases, and multiplying by one million to yield reads per kilobase per million (RPKM) values. Pearson's correlation coefficients

were determined between strains for ORFs that had at least 128 reads between the two datasets (Ingolia et al., 2009)

Supplemental References

Coudert, L., Adjibade, P., and Mazroui, R. (2014). Analysis of translation initiation during stress conditions by polysome profiling. J. Vis. Exp. *87*, doi: 10.3791/51164.

Drost, J., Nonis, D., Eich, F., Leske, O., Damrath, E., Brunt, E.R., Lastres-Becker, I., Heumann, R., Nowock, J., and Auburger, G. (2013). Ataxin-2 modulates the levels of grb2 and SRC but not ras signaling. J. Mol. Neurosci. *51*, 68-81.

Ingolia, N.T., Brar, G.A., Rouskin, S., McGeachy, A.M., and Weissman, J.S. (2012). The ribosome profiling strategy for monitoring translation in vivo by deep sequencing of ribosome-protected mRNA fragments. Nat. Protoc. *7*, 1534-1550.

Ingolia, N.T., Ghaemmaghami, S., Newman, J.R., and Weissman, J.S. (2009). Genome-wide analysis in vivo of translation with nucleotide resolution using ribosome profiling. Science *324*, 218-223.